






# Analytical Conduction Loss Calculation of a MOSFET Three-Phase Inverter Accounting for the Reverse Conduction and the Blanking Time

Alessandro Acquaviva , *Student Member, IEEE*, Artem Rodionov , *Student Member, IEEE*, Anton Kersten , *Student Member, IEEE*, Torbjörn Thiringer , *Senior Member, IEEE*, and Yujing Liu , *Senior Member, IEEE*

**Abstract**—The reverse conduction capability of MOSFETs is beneficial for the efficiency of a three-phase inverter. In this article, analytical expressions in closed form are presented which allow to quickly evaluate the conduction losses, considering the effect of the reverse conduction, and blanking time for both sinusoidal pulsewidth modulation operation with and without third harmonic injection. The losses of a three-phase silicon carbide MOSFET inverter suitable for traction applications are estimated with the proposed method and show good agreement of about 98.5% with measurements, performed with a calorimetric setup.

**Index Terms**—Analytical models, calorimetry, power MOSFET, pulsewidth modulated inverters, traction motor drives.

## I. INTRODUCTION

THE thermal capability and the low switching losses of silicon carbide (SiC) MOSFETs can be beneficial in comparison to classical silicon (Si) IGBTs when used in a three-phase converter [1]–[4]. Available comparisons between SiC MOSFET and Si IGBT based converters show that SiC MOSFETs can achieve a more compact inverter design, while improving the system efficiency [1], [2]. Especially at high switching frequencies and high junction temperatures, the converter efficiency can be increased using SiC MOSFETs [2]–[6]. Furthermore, MOSFET based converters, as described in [7]–[11], have also reduced conduction losses at partial load operation. In [12]–[16], extensive work has been done to derive analytical switching-loss models.

However, the available comparisons in [1]–[9] are mainly based on analytical conduction-loss models in the literature

Manuscript received October 3, 2019; revised January 26, 2020, April 3, 2020, and May 11, 2020; accepted June 5, 2020. Date of publication June 25, 2020; date of current version April 27, 2021. This work was supported by the Swedish Energy Agency. (*Corresponding author: Anton Kersten.*)

The authors are with the Division of Electric Power Engineering at Chalmers, University of Technology, 41296 Gothenburg, Sweden (e-mail: alessandro.acquaviva@chalmers.se; artem@chalmers.se; kersten@chalmers.se; torbjorn.thiringer@chalmers.se; yujing.liu@chalmers.se).

Color versions of one or more of the figures in this article are available online at <https://ieeexplore.ieee.org>.

Digital Object Identifier 10.1109/TIE.2020.3003586

[17]–[20] or provided by semiconductor manufacturers' application manuals [21], [22] for different IGBT and MOSFET converter topologies. These models do not include the effect of the reverse conduction in the MOSFET inverter, also referred to as third quadrant characteristic [23]–[25]. MOSFET devices typically have a body diode that allows for reverse conduction. Additionally, when a negative drain–source voltage is present, the MOSFET channel's conduction can also be controlled by applying a gate–source voltage above the threshold voltage level [26]. In a three-phase inverter, this results in parallel conduction of the diode and MOSFET when output voltage and current differ in sign.

The conventional way of controlling a two-level three-phase inverter is to send a pulsewidth modulation (PWM) signal to the top switch of the inverter leg and the inverted PWM signal to the bottom one with a blanking time in between to prevent a short circuit of the leg [27]. This means that, typically, all MOSFET converters use the reverse conduction capability. An analytical conduction loss model for three-phase SiC MOSFET inverters, which includes the reverse conduction, was first presented in [28]. However, this model is limited to an output PWM signal using a pure sinusoidal reference and the effect of the blanking time is not included. In [29], models are presented for different modulation strategies, however, they do not accurately consider the effect of the current split between the diode and the MOSFET. In [30], the authors have presented analytical expressions to quickly evaluate the conduction losses, taking into account the effect of the reverse conduction and the blanking time. Both sinusoidal PWM operation with and without third harmonic injection, which can also be used for space vector modulation with small error, are derived in a closed form. Further, these analytical expressions have been validated with numerical simulations and it was shown that the loss reduction due to the reverse conduction is significant over a driving cycle [30]. However, all presented models [29]–[31] are lacking experimental validation, which is quite challenging. Because of the high efficiency, and hence low losses, the simple subtraction of output power from input power involves a small relative difference between these quantities, and is therefore prone to large errors and low accuracy. Calorimetry is a recognized means for the direct measurement of losses in power electronics inverters, which can be used to overcome these difficulties [32]–[35].

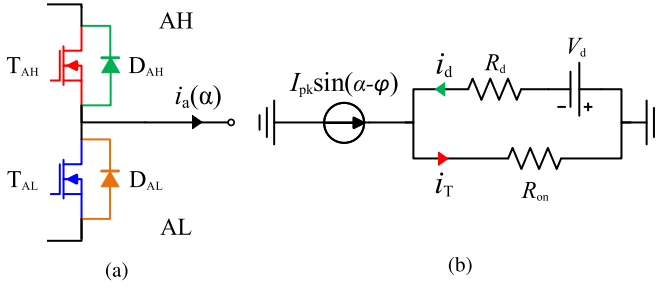


**Fig. 1.** (a) Single inverter leg (half-bridge) of a three-phase inverter. (b) Equivalent circuit of parallel conduction of diode and MOSFET channel in reverse direction [26]. During the reverse conduction  $i_T < 0$ , and, thus, the MOSFET current flows in opposite direction of the red current arrow.

The contribution of this article is to experimentally verify theoretically derived expressions regarding the impact of the reverse conduction on the conduction losses of a MOSFET three-phase inverter. Therefore, this article derives and presents simplified analytical expressions, based on [30], to quickly evaluate the conduction losses in a three-phase MOSFET converter, including the effect of the reverse conduction and the blanking time. A SiC MOSFET three-phase inverter is tested in different operating conditions using a double jacketed calorimeter with a water cooled circuit, resulting in high accuracy of the loss measurements. Thus, the presented loss models are experimentally validated.

## II. CONDUCTION LOSSES CONSIDERING REVERSE CONDUCTION OF MOSFET CHANNEL

The steady-state conduction losses of a three-phase voltage source inverter, utilizing MOSFETs, are evaluated in this article. It is assumed that all three-phase output currents are sinusoidal and balanced. Under this assumption, it is sufficient to calculate the losses for a single inverter leg as shown in **Fig. 1(a)**. Consequently, the result can be extended to the other two legs. The average MOSFET conduction losses can be calculated, approximating the drain source characteristic to an ON-state resistance  $R_{on}$ , as

$$P_{c,T} = \frac{1}{2\pi} \int_0^{2\pi} D(\alpha) R_{on} i_T^2(\alpha) d\alpha \quad (1)$$

where  $\alpha = \frac{2\pi}{T}t$  and  $D$  is the duty cycle. Similarly, the diode conduction losses can be obtained, approximating the forward characteristic to mimic an ON-state resistance  $R_d$  and a constant voltage drop  $V_d$  as

$$P_{c,d} = \frac{1}{2\pi} \int_0^{2\pi} D(\alpha) (R_d i_d^2(\alpha) + V_d i_d(\alpha)) d\alpha. \quad (2)$$

Assuming a naturally sampled PWM sine-triangle modulation, the duty cycle as a function of  $\alpha$  can be defined as

$$D(\alpha) = \frac{1}{2}(1 + M \sin(\alpha)) \quad (3)$$

where  $M$  is the modulation index [17]. When current and voltage in one leg are discordant, either the upper or the lower diode

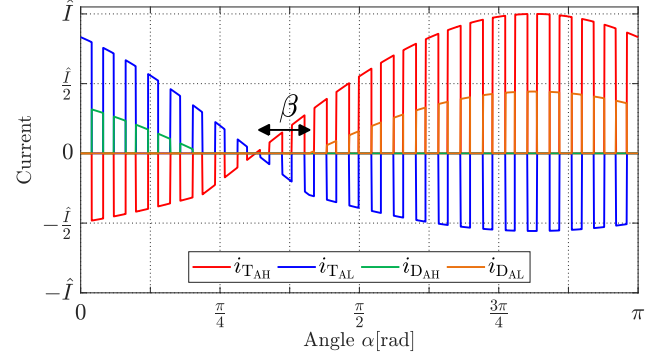


**Fig. 2.** Parallel conduction of diode and MOSFET channel, starting at angle  $\beta$  relative to the zero current crossing.

is forward biased. If the corresponding MOSFET gate–source voltage is above the threshold voltage level, the MOSFET channel conducts in parallel with the diode. Due to the constant voltage drop, the diode will only be forward biased, if the device current times the ON-state resistance  $R_{on}$  is above the diode's threshold voltage  $V_d$ . Thus, it is convenient to define the parallel conduction angle  $\beta$  as

$$\sin(\beta) = \frac{V_d}{R_{on} \hat{I}} \quad (4)$$

shown in **Fig. 2**. For example, when the load current is positive and MOSFET  $T_{AH}$  in **Fig. 1** is provided with a positive gate–source voltage, the phase to neutral voltage will be positive and  $T_{AH}$  will conduct the current

$$i_{T,1}(\alpha) = \hat{I} \sin(\alpha - \varphi) \quad \text{for } -\beta \leq \alpha - \varphi \leq \beta + \pi \quad (5)$$

where  $\varphi$  is the angle of displacement power factor (DPF) and  $\hat{I}$  is the peak value of the phase current. On the other hand, when MOSFET  $T_{AH}$  is OFF, diode  $D_{AL}$  will conduct in parallel with MOSFET  $T_{AL}$ . Therefore, the diode and MOSFET currents during the parallel conduction of  $T_{AH}$  and  $D_{AH}$ , as schematically shown in **Fig. 1(b)**, are calculated as

$$i_{T,2}(\alpha) = \frac{R_d \hat{I} \sin(\alpha - \varphi) - V_d}{R_d + R_{on}} \quad \text{for } \pi + \beta \leq \alpha - \varphi \leq 2\pi - \beta \quad (6)$$

and

$$i_d(\alpha) = -\frac{R_{on} \hat{I} \sin(\alpha - \varphi) + V_d}{R_d + R_{on}} \quad \text{for } \pi + \beta \leq \alpha - \varphi \leq 2\pi - \beta. \quad (7)$$

The integral in (1) can be calculated for the different intervals by defining  $\vartheta = \alpha - \varphi$  as

$$P_{c,T} = \frac{R_{on}}{4\pi} \left( \int_{-\beta}^{\pi+\beta} (1 + M \sin(\vartheta + \varphi)) i_{T,1}^2(\alpha) d\vartheta + \int_{\pi+\beta}^{2\pi-\beta} (1 + M \sin(\vartheta + \varphi)) i_{T,2}^2(\alpha) d\vartheta \right). \quad (8)$$

Inserting (5) and (6) in (8), the conduction losses can be expressed as

$$P_{c,T} = \frac{R_{on}}{4\pi} \left( \int_{-\beta}^{\pi+\beta} (1 + M\sin(\vartheta + \varphi)) \hat{I}^2 \sin^2(\vartheta) d\vartheta + \int_{\pi+\beta}^{2\pi-\beta} (1 + M\sin(\vartheta + \varphi)) \left( \frac{R_d \hat{I} \sin(\vartheta) - V_d}{R_d + R_{on}} \right)^2 d\vartheta \right). \quad (9)$$

Similarly, the integral in (2) can be expressed as

$$P_{c,d} = \frac{1}{4\pi} \int_{\pi+\beta}^{2\pi-\beta} (1 + M\sin(\vartheta + \varphi)) (R_d i_d^2(\alpha) + V_d i_d(\alpha)) d\vartheta. \quad (10)$$

Inserting (7) in (10) yields

$$P_{c,d} = \frac{1}{4\pi} \int_{\pi+\beta}^{2\pi-\beta} (1 + M\sin(\vartheta + \varphi)) \times \left[ R_d \left( \frac{R_{on} \hat{I} \sin(\alpha - \varphi) + V_d}{R_d + R_{on}} \right)^2 - V_d \left( \frac{R_{on} \hat{I} \sin(\alpha - \varphi) + V_d}{R_d + R_{on}} \right) \right] d\vartheta. \quad (11)$$

A third harmonic can be added to the reference voltage in order to achieve a higher value of the fundamental output voltage. Typically, the optimal value is 1/6 of  $M$ , allowing the output voltage to be increased by up to 15% without reaching the overmodulation region. The duty cycle expression in the integral to calculate the losses when a third harmonic is added to the reference is

$$D(\alpha) = \frac{1}{2} (1 + M\sin(\alpha) + \frac{1}{6} M\sin(3\alpha)). \quad (12)$$

The complete expressions with the integrals in (8) and (11) and considering the third harmonic injection (12) are reported in the Appendix.

### A. Effect of the Blanking Time

Because of the finite turn-ON and turn-OFF times, associated with any type of semiconductor switch, a delay time, often referred to as blanking time  $t_{bl}$  between the conduction of the upper and lower switch of the same inverter leg must be implemented in order to avoid a shoot-through. During the blanking time, only the diode is conducting the current. The effect of the blanking time is shown in Fig. 3. Its effect on the MOSFET conduction loss calculation can be accounted by defining an equivalent duty cycle

$$D_{eq}(\alpha) = D(\alpha) - t_{bl} f_{sw} = \frac{1}{2} (1 - 2t_{bl} f_{sw} + M\sin(\alpha)) \quad (13)$$

where  $f_{sw}$  is the switching frequency. Negative duty cycle values are not to be considered, so the condition

$$1 - 2t_{bl} f_{sw} + M\sin(\alpha) > 0 \quad (14)$$

must be verified in the case of a sinusoidal reference voltage. In the case with 1/6 third harmonic injection the condition to

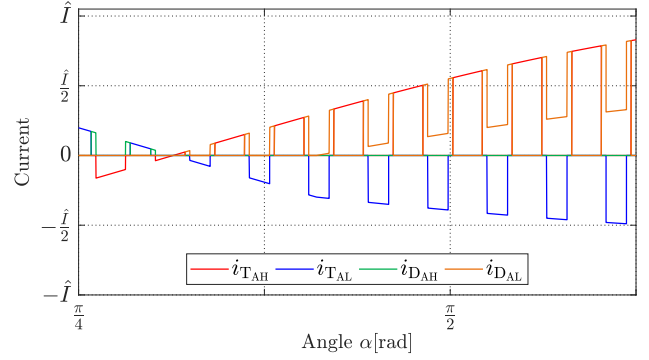


Fig. 3. Effect of the blanking time on the diode and MOSFET current.

fulfill is

$$1 - 2t_{bl} f_{sw} + M\sin(\alpha) + 1/6 M\sin(3\alpha) > 0. \quad (15)$$

For values of  $M$  close to the boundary of the overmodulation region, the method of using an equivalent duty cycle should be applied carefully. Negative duty cycle values are to be avoided. Since the diode is conducting the whole current during the blanking time, the average conduction losses in (11) must be extended by the addition of

$$\frac{1}{2\pi} \int_{\pi}^{2\pi} 2t_{bl} f_{sw} \left( R_d \hat{I}^2 \sin^2(\vartheta) - \hat{I} \sin(\vartheta) V_d \right) d\vartheta \quad (16)$$

which results in

$$t_{bl} f_{sw} \hat{I} \left( \frac{1}{2} \hat{I} R_d + \frac{2}{\pi} V_d \right). \quad (17)$$

While (9) and (11) have been derived without introducing any approximation, the formulas including the blanking time have some degree of approximation. Using an equivalent duty cycle as in (13) means a reduction of the current conduction interval with two times the blanking time. However, the blanking time intervals are not specifically placed at the beginning or the end of the reverse conduction, but are considered averaged over the whole electrical period, introducing a small error. Nevertheless, the entity of this error is still negligible and the equivalent duty cycle is very accurate in estimating the losses including the effect of blanking time as shown in [30].

Again the complete analytical expressions of the conduction losses, including the effect of the blanking time, are reported in the Appendix.

### B. Switching Losses

In order to evaluate the overall efficiency of the three-phase inverter, the switching losses need to be considered as well. The device's data sheet usually provides the switching losses as a function of the device current for certain voltage levels. Thus, the switching losses for one semiconductor switch can be calculated, taking every switching event into account, by a

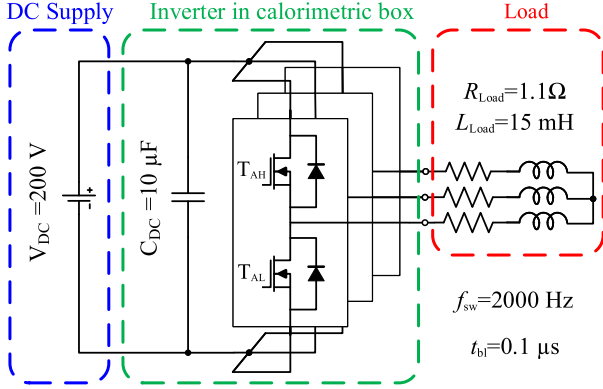


Fig. 4. Schematic operation of the inverter setup, using an  $RL$ -load. The low switching frequency and the low dc-link voltages reduce the switching losses.

look-up table approach, as

$$P_{sw} = \frac{\sum_{j=1}^{n=T_1 f_{sw}} (E_{on,j}(i_T(t)) + E_{off,j}(i_T(t)) + E_{rr,j})}{T_1} \quad (18)$$

where  $T_1$  is the fundamental period of the output voltage and  $E_{rr}$  is the reverse recovery loss. The switching losses,  $E_{on}(i_T)$  and  $E_{off}(i_T)$ , can be scaled according to the dc-link voltage as

$$E_{on/off}(i_T) = \left( \frac{V_{DS}}{V_{DC,ref}} \right)^{K_{v,on/off}} \quad (19)$$

The value of  $K_{v,on/off}$  is typically about 1.4 [36] and can be obtained from the supplier's data sheet through interpolation. According to [22], the switching loss calculation can be simplified by expressing the ac current through an equivalent dc current as

$$I_{DC} = \frac{\hat{I}}{\pi} = i_T. \quad (20)$$

Thus, the switching losses can be estimated as

$$P_{sw} = f_{sw} (E_{on}(I_{DC}) + E_{off}(I_{DC}) + E_{rr}). \quad (21)$$

Having the MOSFET turning ON and OFF during reverse conduction would in theory increase the switching losses. However, due to the fact that the diode is conducting in parallel or is conducting during the blanking time, the voltage across the MOSFET is forced to  $V_d + R_d \hat{I}$  during the beginning of the switching transient, achieving quasi zero-voltage-switching (ZVS) [12], [37]. Therefore, the switching losses of the MOSFET during reverse conduction are negligible.

### III. EXPERIMENTAL VALIDATION

To experimentally validate the conduction-loss models derived in Section II, a SiC MOSFET inverter was operated with and without reverse conduction using a calorimetric box, as schematically shown in Fig. 4. In this section, the experimental setup is described and the loss measurements are presented and compared with the analytical models.

TABLE I  
EQUIPMENT LIST

Device	Manufacturer	Model
SiC module 1.2 kV/50 A	Wolfspeed	CCS050M12CM2 [38]
SiC gate driver board	Wolfspeed	CGD15FB45P1 [39]
2 DC link capacitors 5 μF	Vishay	MKP386M550125YT4
4W-PT100	RS PRO	25mm x 4mm Probe
Acquisition unit	Fluke	Hydra 2620A
Pump	Shenzhen	LabN6

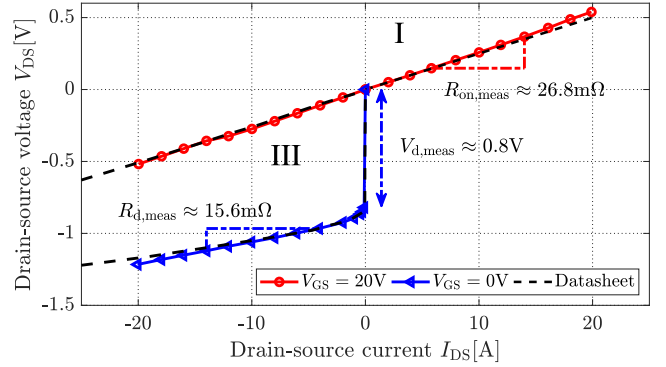


Fig. 5. Measured MOSFET and diode characteristic of the chosen SiC MOSFET inverter. Reverse conduction is also shown.

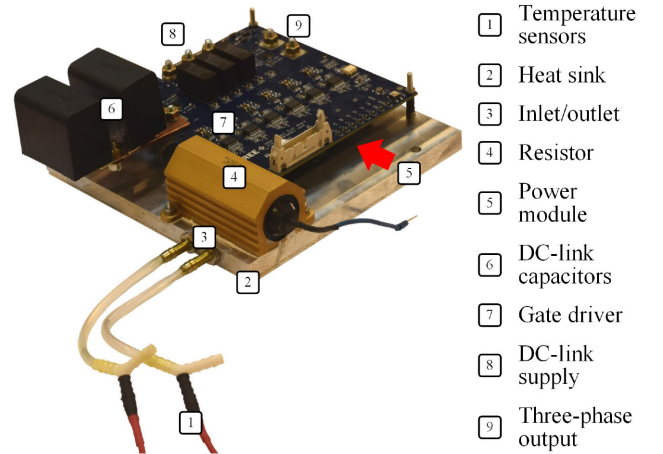
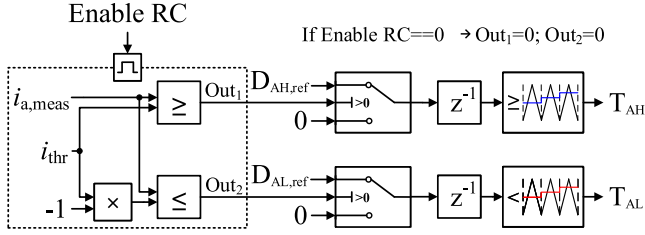


Fig. 6. Three-phase inverter prototype and calibration resistor mounted on the water cooled heatsink.

#### A. Case Study and Setup Description

A SiC MOSFET inverter was built using one of Cree's six-pack three-phase modules, including the custom gate driver board, listed in Table I. The MOSFETs' and diodes' voltage drop, including the effect of the reverse conduction, were experimentally characterized at ambient temperature for different drain-source current levels, as can be seen in Fig. 5. The module, together with a 220-Ω calibration resistor with a maximum power dissipation of 100 W, was mounted on a water cooled heat sink as shown in Fig. 6.

The PWM signals were generated using a DSpace DS1006 processor board and DS5202 FPGA base board. A program was implemented to be able to enable the reverse conduction, with



**Fig. 7.** Schematic description to disable the reverse conduction by keeping the gate switched OFF, if the phase current exceeds the threshold value  $i_{thr}$ .

- |                 |                   |                    |
|-----------------|-------------------|--------------------|
| 1 dSPACE system | 3 Flow pump       | 5 Calorimetric box |
| 2 Oscilloscope  | 4 Water reservoir | 6 RL-load          |

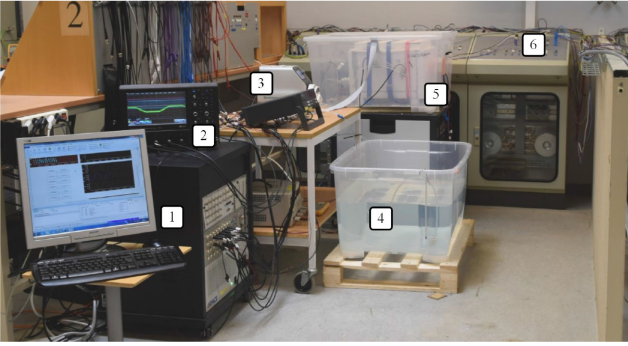


**Fig. 8.** Actual test setup environment with calorimetric box, water reservoir, data acquisition, and control unit.

reverse conduction (W-RC), and disable the reverse conduction, with-out reverse conduction (WO-RC), by either providing a high or a low gate signal to the corresponding SiC MOSFET when voltage and current are of opposite sign. A schematic description of the program is presented in Fig. 7. The complete laboratory setup is shown in Fig. 8. The double jacketed calorimetric box, as described in [40], has an inner and an outer air chamber. Having two chambers reduces the leakage heat through the box walls. The inverter and heatsink were fitted inside the calorimetric box with high-resolution temperature sensors (4-wire PT100) at the water inlet and outlet. The pump used in the setup is a medical grade pump, see Table I, able to operate with a high accuracy at very low flow rates. A low flow rate of  $200 \text{ mL min}^{-1}$  was chosen in order to increase the outlet to inlet water temperature difference and have a good reading accuracy of the temperature sensors. This is necessary when measuring losses in the range of 10–30 W. The inverter's losses were measured using the thermal steady-flow energy equation (SFEE)

$$P_{\text{loss}}(1 - \sigma_{\text{th}}) = c_p \dot{V} \rho \Delta T \quad (22)$$

where  $\sigma_{\text{th}}$  is the calorimetric box's leakage factor,  $c_p$  is the heat capacity at constant pressure,  $\dot{V}$  is the volumetric flow rate,  $\rho$  is the volumetric mass density, and  $\Delta T$  is the temperature difference between the inlet and the outlet. To determine the heat leakage conducted through the cables and the walls, a

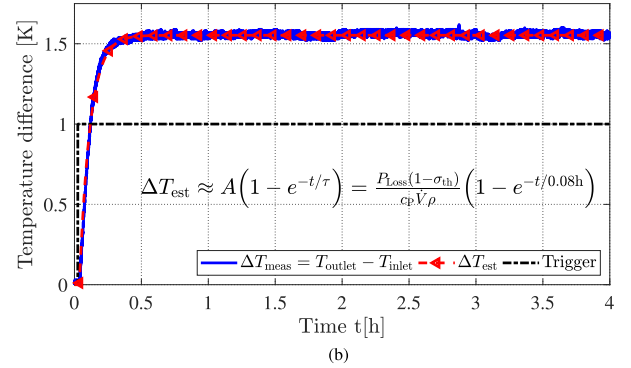
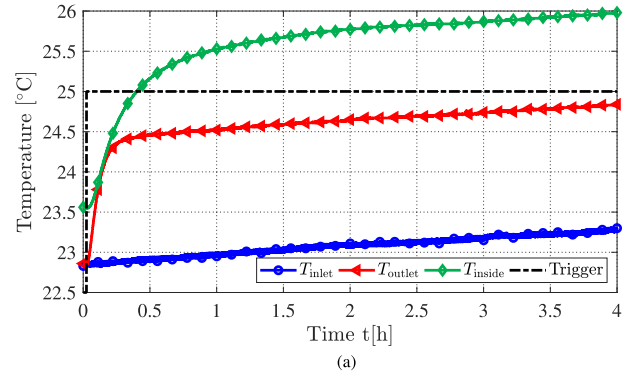


**Fig. 9.** Transient temperature profiles using a flow rate of  $200 \text{ mL min}^{-1}$  for about 25 W of injected power. (a) Temperature profiles of the water inlet, water outlet, and the air inside the box. (b) Water temperature difference between the outlet and the inlet, both measured and estimated.

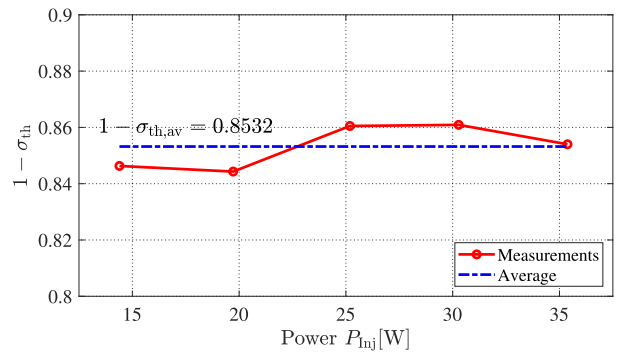


**Fig. 10.** Calorimetric box's leakage factor measured for different power levels of injected dc power using the calibration resistor.

specific loss was injected, using the calibration resistor, and compared with the measured losses, derived from the cooling circuit. Fig. 9 shows the calibration measurements using an injected power dissipation in the resistor of about 25 W. After an initial transient, the absolute temperatures inside the box were rising with a constant slope due to the fact that the inlet water temperature comes from a water reservoir, which was slowly warming up with time. Regardless, the coolant outlet to inlet temperature difference becomes constant after the first transient, which can be considered as a quasi-steady state for the loss evaluation. The calibration results for different levels of injected power dissipation are depicted in Fig. 10. The leakage factor is

fairly constant within the chosen dissipated power range, thus the average value was applied to the measurements on the inverter.

### B. Loss Measurements

The setup, as presented in Figs. 4 and 8, was used to evaluate the conduction losses for both cases, W-RC and WO-RC. The switching frequency of 2 kHz and the dc-link voltage of 200 V were selected in order to focus on the conduction losses by keeping the switching losses low, as the conduction losses are not dependent on the dc-link voltage as shown in (9) and (11). Furthermore, using a switching frequency of 2 kHz and considering the proper modulation of the injected third harmonic component, output fundamental frequencies up to 66.67 Hz can be synthesized [27], while generating some audible noise. In an actual application, it is beneficial to use a switching frequency of at least 20 kHz, to avoid the audible noise. A fixed RL-load was applied on the output and the power factor was varied by changing the fundamental frequency. To adjust the three-phase output current's amplitude, a current controller using loop shaping, as described in [27] and [41] was implemented. The gate driver board inside the calorimetric box was generating additional losses, which were accounted by the measured supply power.

At first, the inverter's output current amplitude was controlled to about 20 A at a frequency of 50 Hz. The high-side and the low-side gate signals together with the output current and the voltage reference of the measurements for one of the three phases are presented in Fig. 11 for the W-RC case and in Fig. 12 for the WO-RC case.

The corresponding temperature difference between the outlet and the inlet of the calorimetric box can be seen in Fig. 13. In time intervals of about 1 h, the inverter was alternately operated with and without reverse conduction. It can be noted that the effect of the reverse conduction has a significant impact on the inverter losses.

The loss comparison between both cases, W-RC and WO-RC, at thermal steady state are presented in Fig. 14. The measured auxiliary losses of approximately (2.8 W) are from the gate driver board. Theoretically, these are dependent on the switching frequency ( $\Delta P_{Aux} \approx 33 \mu\text{WHz}^{-1}$ [39]). The difference of the effective gate driver switching frequency between the cases W-RC and WO-RC was about 1 kHz, which should result in a theoretical, auxiliary loss difference of about 33 mW. In practice, however, there was no difference in the measured auxiliary power. The switching losses were quantified to be approximately 0.2 W, for both W-RC and WO-RC. The switching and the auxiliary losses are added to the conduction losses calculated with the analytical model and compared with the total losses from the calorimetric measurement showing a very good agreement. Considering the case with enabled reverse conduction, the presented analytical expressions show an agreement of approximately 98.5% in comparison to the measured losses. Even when using a 1200 V device with a high ON-state resistance  $R_{on}$  and an antiparallel Schottky diode with a low forward drop  $V_d$ , there is a significant difference between the cases W-RC and WO-RC at partial load operation.

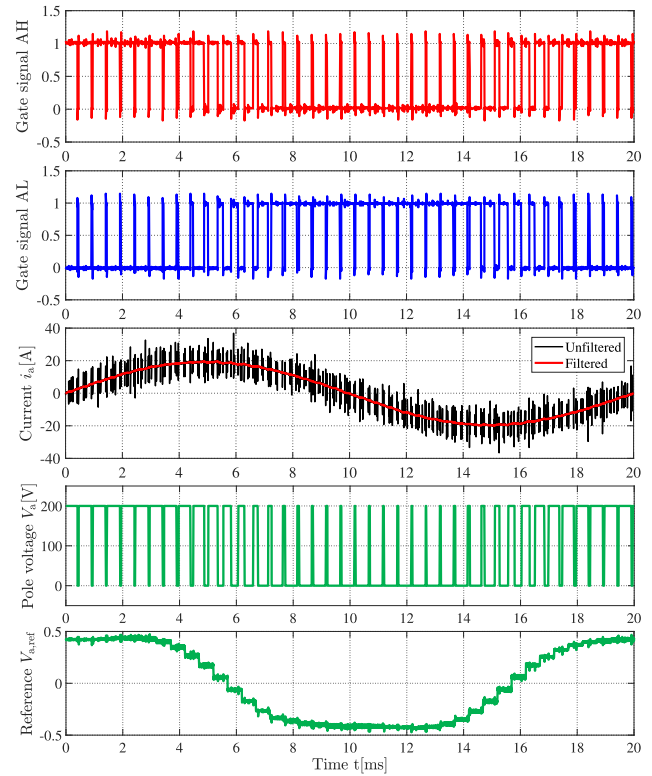


Fig. 11. Gate signals, output current, pole voltage, and reference voltage with enabled reverse conduction (W-RC) for one of the three phases (pole voltage signal is simulated, all other signals are measured).

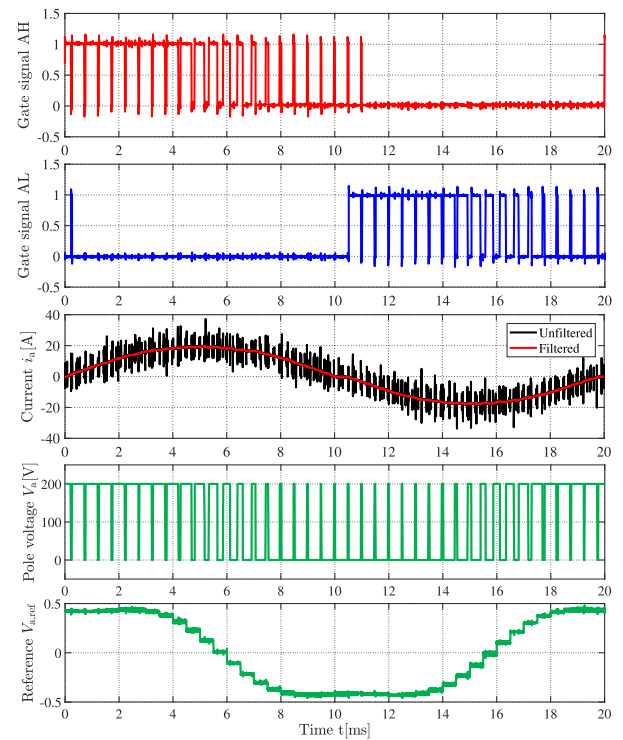


Fig. 12. Gate signals, output current, pole voltage and reference voltage with disabled reverse (WO-RC) conduction for one of the three phases (pole voltage signal is simulated, all other signals are measured).

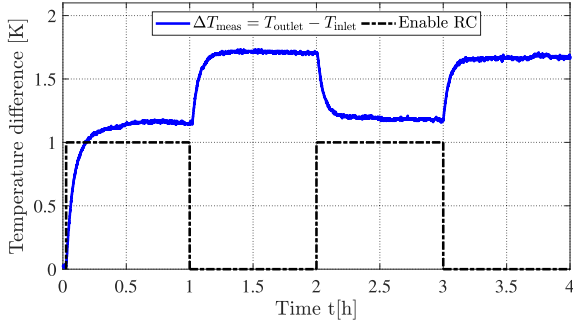


Fig. 13. Measured water temperature difference between the outlet and the inlet with alternately enabled and disabled reverse conduction for a current amplitude of 20 A at 50 Hz.

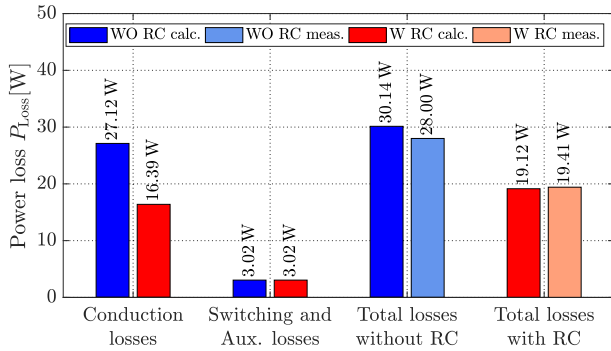


Fig. 14. Comparison of estimated losses, using the analytical models, and measured losses for a current amplitude of 20 A at 50 Hz.

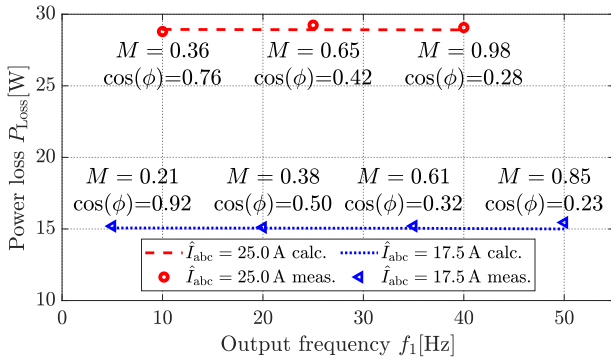


Fig. 15. Comparison of estimated losses, using the analytical model, and measured losses for different operating points with enabled reverse conduction.

The same procedure was repeated for several operating points (all W-RC), varying the frequency of the fundamental (and consequently the power factor) and the amplitude of the output current. The results are presented in Fig. 15. Similarly as before, the losses measured with the calorimetric method match very well with the ones estimated using the analytical models presented in this article.

#### IV. COMPARISON OF THE PROPOSED METHOD

As experimentally shown, the conduction-loss models described in [17]–[20] and the semiconductor manufacturers'

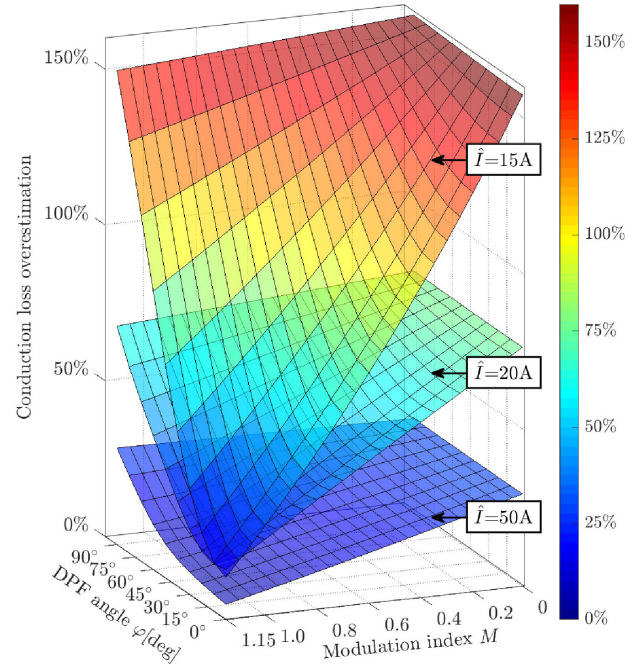


Fig. 16. Overestimation of the conduction losses when using the method described in Semikron's application manual [21] in comparison to the presented method for the SiC MOSFET three-phase inverter of Cree[38].

applications manuals [21], [22] overestimate the conduction losses of a three-phase inverter when using Si and SiC MOSFETs instead of IGBTs. Fig. 16 depicts the overestimation of the conduction losses proposed in [21] in comparison to the model presented in (23) to (30) relative to the modulation index  $M$  and the DPF angle  $\varphi$  for different output current amplitudes. For the calculations, the parameters of the SiC MOSFET power module [38], determined from the measured characteristic in Section II, are used. As can be seen, the relative differences become smaller for larger current amplitudes. For a fixed current amplitude, the overestimation becomes the highest at low modulation index and pure inductive DPF and the lowest at a high modulation index and unity DPF. For the depicted current amplitudes of 15 and 50 A, the relative overestimation varies from 13.5 to 159.3% and 4.9 to 29.8%, respectively.

#### A. Practical Selection of MOSFETs for Three-Phase Inverters Used for Drive Applications

When choosing a MOSFET for a drive application, its rated blocking voltage should be sufficiently higher than the voltage at which it will be actually used in order to withstand the overvoltages caused by each switching event [5], [42]. For example in electric vehicles (EVs), typical dc-link voltages are either 400 V or even 800 V, which leads to a blocking voltage selection of 600 to 650 V or 1200 V, respectively [43], [44]. This corresponds to a design factor of about 1.5 ( $V_{Block}/V_{DC}$ ). Including a safety margin, the MOSFET's maximum drain current should comply with the maximum operating current [5]. The switching frequency should be selected in accordance with

the application and design optimization. For example, to ensure a proper current control it is reasonable to select a switching frequency, which is at least ten times higher than the maximum fundamental frequency [27]. For an EV, the electric motor is typically operated at fundamental frequencies up to about 1 kHz and, thus, a switching frequency of 10 kHz is often selected [41]. If the audible noise needs to be reduced as well, the switching frequency could be increased above 20 kHz [45], [46]. For example, when dealing with grid connected inverters, it might be more beneficial for the overall system design to choose an even higher switching frequency ( $f_{sw} \gg 20$  kHz) to reduce passive components, as for example the grid filter [5], [47]. This in turn would result in a higher portion of the switching losses in relation to the total losses. Subsequently, when considering different MOSFETs, it must be ensured that the sum of the switching and conduction losses does not exceed the maximum permissible power dissipation of the MOSFET and the temperature rise due to the heating should be kept within the specified temperature boundaries, including the application of necessary cooling [42], [48]. The switching losses can be estimated by (18) to (21) using a lookup-table approach with data-sheet values or measurement values obtained from double-pulse tests [49]. The conduction losses can be estimated using (23) to (30). Simple thermal models can be used to estimate the junction temperature of the MOSFET [42], [48].

Since the rated operating point is usually used for the MOSFET selection and circuit design, the difference between the estimated conduction losses, exemplified in comparison to [21] corresponds only to a few percent, as can be seen in Fig. 16. However, the effect of the presented conduction loss estimation becomes more beneficial when considering also the actual operating range throughout the inverter's lifetime, as variable speed drives, e.g., pumps or air compressors are often operated at partial load [50]. In such cases, the properties of the body (or the antiparallel) diode are of less importance as the MOSFET channel is mainly conducting the current in reverse conduction mode. Hence, it might be beneficial to motivate a higher investment cost for a SiC MOSFET inverter with a low ON-state resistance  $R_{on}$  in comparison to a cheap IGBT inverter [5], [7] considering that the increased energy cost savings throughout the lifetime and that the total energy and acquisition costs typically correspond to about 80% and 9% of the total costs, respectively [50].

## V. CONCLUSION

This article presented analytical models to quickly evaluate the conduction losses of a three-phase MOSFET inverter including the effect of the reverse conduction. These models can be used as a quick and accurate tool during the inverter design process to evaluate the inverter efficiency and to perform thermal evaluations.

The proposed equations have been experimentally validated. A SiC MOSFET inverter for traction applications has been tested for different operating conditions and the losses were measured using a calorimetric setup. The measured losses have been compared with the proposed analytical models showing good agreement.

A calculated comparison of the presented method with [21] shows that the available methods for IGBT inverters overestimate the conduction losses when used for MOSFET inverters, especially at partial load operation.

This allows the conclusion that the negligence of the reverse conduction can lead to significant errors in the conduction loss estimation, which might result in an overdimensioned cooling system.

## APPENDIX

$$A = \begin{cases} 1, & \text{for } t_{bl} = 0 \\ 1 - 2t_{bl}f_{sw}, & \text{for } t_{bl} > 0 \end{cases} \quad (23)$$

$$B = \frac{\pi}{2} + \beta - \frac{\sin(2\beta)}{2} \quad (24)$$

$$C = \cos(\beta) - \frac{\cos^3(\beta)}{3} \quad (25)$$

$$D = 2M\cos(\varphi). \quad (26)$$

Average MOSFET conduction losses (one switch), using sinusoidal voltage reference

$$\begin{aligned} P_{c,T} = & \frac{R_{on}\hat{I}^2}{4\pi}(AB + CD) \\ & + \frac{R_{on}}{4\pi(R_{on} + R_d)^2} \left( \hat{I}^2 R_d^2 (A(\pi - B) - CD) \right. \\ & + V_d^2 ((\pi - 2\beta)A - D\cos(\beta)) + \hat{I}R_d V_d (4A\cos(\beta) \\ & \left. - (\pi - B)D) \right). \end{aligned} \quad (27)$$

Average diode conduction losses (one diode), using sinusoidal voltage reference

$$\begin{aligned} P_{c,d} = & \frac{R_d}{4\pi(R_{on} + R_d)^2} \left( R_{on}^2 \hat{I}^2 (\pi - B - CD) \right. \\ & \left. + V_d^2 (\pi - 2\beta - D\cos(\beta)) - R_{on} \hat{I} V_d (4\cos(\beta) - (\pi - B)D) \right) \\ & - \frac{V_d}{4\pi(R_{on} + R_d)} \left( \frac{1}{2} R_{on} \hat{I} (\pi - B)D + 2R_{on} \hat{I} \cos(\beta) \right. \\ & \left. - V_d (\pi - 2\beta) + V_d D \cos(\beta) \right) + t_{bl} f_{sw} \hat{I} \left( \frac{1}{2} \hat{I} R_d + \frac{2}{\pi} V_d \right). \end{aligned} \quad (28)$$

Additional average MOSFET conduction losses (one switch), using 1/6 third harmonic injection (to be added to (27))

$$\begin{aligned} & \frac{MR_{on}\hat{I}^2}{60\pi} \cos(3\varphi) (4\sin^4(\beta)\cos(\beta) + C) \left( \frac{R_d^2}{(R_{on} + R_d)^2} - 1 \right) \\ & - \frac{MV_d^2}{36\pi(R_{on} + R_d)} \cos(3\varphi) \cos(3\beta) \left( \frac{R_{on}}{(R_{on} + R_d)} \right) \\ & - \frac{MR_{on}\hat{I}R_d V_d}{24\pi(R_{on} + R_d)^2} \cos(3\varphi) \left( \frac{\sin(4\beta)}{2} - \sin(2\beta) \right). \end{aligned} \quad (29)$$



Additional average diode conduction losses (one diode), using 1/6 third harmonic injection (to be added to (28)):

$$\begin{aligned} & \frac{M\hat{I}^2 R_d}{60\pi} \cos(3\varphi) (4\sin^4(\beta)\cos(\beta) + C) \left( \frac{R_{on}^2}{(R_{on} + R_d)^2} \right) \\ & - \frac{MR_{on}\hat{I}V_d}{48\pi(R_{on} + R_d)} \left( \cos(\varphi) \left[ \sin(2\varphi)\cos(2\beta) \right. \right. \\ & \left. \left. - \frac{\sin(4\varphi)\cos(4\beta)}{2} \right] \right) \\ & - \sin(\varphi) \left[ \sin(2\varphi)\cos(2\beta) - \frac{\cos(4\varphi)\cos(4\beta)}{2} \right] \\ & + \frac{MV_d^2}{36\pi(R_{on} + R_d)} \cos(3\varphi)\cos(3\beta) \left( 1 - \frac{R_d}{(R_{on} + R_d)} \right) \\ & + \frac{MR_{on}\hat{I}R_d V_d}{24\pi(R_{on} + R_d)^2} \cos(3\varphi) \left( \frac{\sin(4\beta)}{2} - \sin(2\beta) \right). \quad (30) \end{aligned}$$

## REFERENCES

- [1] T. Zhao, J. Wang, A. Q. Huang, and A. Agarwal, "Comparisons of SiC mosfet and Si IGBT based motor drive systems," in *Proc. IEEE Ind Appl. Annu. Meeting*, Sep. 2007, pp. 331–335.
- [2] H. Zhang and L. M. Tolbert, "Efficiency impact of silicon carbide power electronics for modern wind turbine full scale frequency converter," *IEEE Trans. Ind. Electron.*, vol. 58, no. 1, pp. 21–28, Jan. 2011.
- [3] M. Chinthavali, P. Otaduy, and B. Ozpineci, "Comparison of Si and SiC inverters for IPM traction drive," in *Proc. IEEE Energy Convers. Congr. Expo.*, Sep. 2010, pp. 3360–3365.
- [4] H. Zhang, L. M. Tolbert, and B. Ozpineci, "Impact of SiC devices on hybrid electric and plug-in hybrid electric vehicles," *IEEE Trans. Ind Appl.*, vol. 47, no. 2, pp. 912–921, Mar. 2011.
- [5] S. Tiwari, O. Midtgard, and T. M. Undeland, "SiC MOSFETs for future motor drive applications," in *Proc. 18th Eur. Conf. Power Electron. Appl.*, Sep. 2016, pp. 1–10.
- [6] J. Biela, M. Schweizer, S. Waffler, and J. W. Kolar, "SiC versus Si-evaluation of potentials for performance improvement of inverter and dc–dc converter systems by SiC power semiconductors," *IEEE Trans. Ind. Electron.*, vol. 58, no. 7, pp. 2872–2882, Jul. 2011.
- [7] T. Bertelshofer, R. Horff, A. Maerz, and M. Bakran, "A performance comparison of a 650 V Si IGBT and SiC MOSFET inverter under automotive conditions," in *Proc. PCIM Eur. Int. Exhib. Conf. Power Electron., Intell. Motion, Renewable Energy Manage.*, May 2016, pp. 1–8.
- [8] F. Chang, O. Iliina, M. Lienkamp, and L. Voss, "Improving the overall efficiency of automotive inverters using a multilevel converter composed of low voltage Si MOSFETs," *IEEE Trans. Power Electron.*, vol. 34, no. 4, pp. 3586–3602, Apr. 2019.
- [9] X. She, A. Q. Huang, Ó. Lucía, and B. Ozpineci, "Review of silicon carbide power devices and their applications," *IEEE Trans. Ind. Electron.*, vol. 64, no. 10, pp. 8193–8205, Oct. 2017.
- [10] A. Kersten, E. Grunditz, and T. Thiringer, "Efficiency of active three-level and five-level NPC inverters compared to a two-level inverter in a vehicle," in *Proc. 20th Eur. Conf. Power Electron. Appl.*, Sep. 2018, pp. P.1–P.9.
- [11] A. Kersten *et al.*, "Inverter and battery drive cycle efficiency comparisons of CHB and MMSP traction inverters for electric vehicles," in *Proc. 21st Eur. Conf. Power Electron. Appl.*, Sep. 2019, pp. P.1–P.12.
- [12] Y. Ren, M. Xu, J. Zhou, and F. C. Lee, "Analytical loss model of power MOSFET," *IEEE Trans. Power Electron.*, vol. 21, no. 2, pp. 310–319, Mar. 2006.
- [13] K. Vechalapu, S. Bhattacharya, E. Van Brunt, S. Ryu, D. Grider, and J. W. Palmour, "Comparative evaluation of 15-kV SiC MOSFET and 15-kV SiC IGBT for medium-voltage converter under the same DV/DT conditions," *IEEE J. Emerg. Sel. Topics Power Electron.*, vol. 5, no. 1, pp. 469–489, Mar. 2017.
- [14] J. Fu, Z. Zhang, Y. Liu, and P. C. Sen, "MOSFET switching loss model and optimal design of a current source driver considering the current diversion problem," *IEEE Trans. Power Electron.*, vol. 27, no. 2, pp. 998–1012, Feb. 2012.
- [15] K. Peng, S. Eskandari, and E. Santi, "Analytical loss model for power converters with SiC MOSFET and SiC Schottky diode pair," in *Proc. IEEE Energy Convers. Congr. Expo.*, Sep. 2015, pp. 6153–6160.
- [16] M. Rodríguez, A. Rodríguez, P. F. Miaya, D. G. Lamar, and J. S. Zúñiga, "An insight into the switching process of power MOSFETs: An improved analytical losses model," *IEEE Trans. Power Electron.*, vol. 25, no. 6, pp. 1626–1640, Jun. 2010.
- [17] J. W. Kolar, H. Ertl, and F. C. Zach, "Influence of the modulation method on the conduction and switching losses of a PWM converter system," *IEEE Trans. Ind Appl.*, vol. 27, no. 6, pp. 1063–1075, Nov. 1991.
- [18] L. Mestha and P. Evans, "Analysis of on-state losses in PWM inverters," *IEEE Proc. B—Electric. Power Appl.*, vol. 136, no. 4, pp. 189–195, Jul. 1989.
- [19] F. Casanellas, "Losses in PWM inverters using IGBTs," *IEEE Proc.—Electric. Power Appl.*, vol. 141, no. 5, pp. 235–239, 1994.
- [20] M. H. Bierhoff and F. W. Fuchs, "Semiconductor losses in voltage source and current source IGBT converters based on analytical derivation," in *Proc. IEEE 35th Annu. Power Electron. Specialists Conf.*, Jun. 2004, vol. 4, pp. 2836–2842.
- [21] A. Wintrich, U. Nicolai, W. Tursky, and T. Reimann, *Application Manual Power Semiconductors - Semikron*. Ilmenau: ISLE Verlag., 2015.
- [22] D. Graovac, M. Purschel, and A. Kiep, "Mosfet power losses calculation using the data-sheet parameters," *Infineon Application Note*, vol. 1, 2006.
- [23] R. Callanan, J. Rice, and J. Palmour, "Third quadrant behavior of SiC MOSFETs," in *Proc. 28th Annu. IEEE Appl. Power Electron. Conf. Expo.*, Mar. 2013, pp. 1250–1253.
- [24] J. Rodríguez, D. G. Lamar, J. Roig, A. Rodríguez, and F. Bauwens, "Improving the third quadrant operation of superjunction MOSFETs by using the cascode configuration," *IEEE Trans. Power Electron.*, vol. 34, no. 3, pp. 2726–2738, Mar. 2019.
- [25] G. Wang, F. Wang, G. Magai, Y. Lei, A. Huang, and M. Das, "Performance comparison of 1200V 100A SiC MOSFET and 1200V 100A silicon IGBT," in *Proc. IEEE Energy Convers. Congr. Expo.*, Sep. 2013, pp. 3230–3234.
- [26] D. Jiang, R. Burgos, F. Wang, and D. Boroyevich, "Temperature-dependent characteristics of SiC devices: Performance evaluation and loss calculation," *IEEE Trans. Power Electron.*, vol. 27, no. 2, pp. 1013–1024, Feb. 2012.
- [27] L. Harnefors, *Control of Variable-Speed Drives*. Applied Signal Processing and Control, Dept. Electron., Mälardalen Univ., 2002.
- [28] J. Rabkowski and T. Platek, "Comparison of the power losses in 1700V Si IGBT and SiC MOSFET modules including reverse conduction," in *Proc. 17th Eur. Conf. Power Electron. Appl.*, 2015, pp. 1–10.
- [29] G. Su, "Loss modeling for SiC MOSFET inverters," in *Proc. IEEE Vehicle Power Propulsion Conf.*, Aug. 2018, pp. 1–6.
- [30] A. Acquaviva and T. Thiringer, "Energy efficiency of a SiC MOSFET propulsion inverter accounting for the MOSFET's reverse conduction and the blanking time," in *Proc. 19th Eur. Conf. Power Electron. Appl.*, Sep. 2017, pp. P.1–P.9.
- [31] J. Rabkowski and T. Platek, "Comparison of the power losses in 1700V Si IGBT and SiC MOSFET modules including reverse conduction," in *Proc. 17th Eur. Conf. Power Electron. Appl.*, Sep. 2015, pp. 1–10.
- [32] S. D. J. Weier, M. A. Shafi, and R. A. McMahon, "Precision calorimetry for the accurate measurement of losses in power electronic devices," in *Proc. IEEE Ind. Appl. Soc. Annu. Meeting*, Oct. 2008, pp. 1–7.
- [33] S. D. J. Weier, R. A. McMahon, and P. D. Malliband, "Calorimetry for power electronics," in *Proc. 41st Int. Univ. Power Eng. Conf.*, Sep. 2006, vol. 2, pp. 608–612.
- [34] D. Christen, U. Badstuebner, J. Biela, and J. W. Kolar, "Calorimetric power loss measurement for highly efficient converters," in *Proc. Int. Power Electron. Conf.*, Jun. 2010, pp. 1438–1445.
- [35] N. Simpson and A. N. Hopkins, "An accurate and flexible calorimeter topology for power electronic system loss measurement," in *Proc. IEEE Int. Elect. Mach. Drives Conf.*, May 2017, pp. 1–6.
- [36] E. Grunditz, *Design and Assessment of Battery Electric Vehicle Powertrain, With Respect to Performance, Energy Consumption and Electric Motor Thermal Capability*. Gothenburg, Sweden: Chalmers Univ. Technol., 2016.
- [37] N. Fritz, M. Rashed, and C. Klumpner, "Power density optimization of a DC/DC converter for an aircraft supercapacitors energy storage," in *Proc. IEEE Int. Conf. Elect. Syst. Aircr., Ship Propulsion Road Veh. Int. Transp. Electrification Conf.*, Nov. 2018, pp. 1–9.
- [38] Cree Wolfspeed, "SiC Power Module, 1200V, 50A, Six-pack - CCS050M12CM2," [Online]. Available: <https://www.wolfspeed.com/media/downloads/189/CCS050M12CM2.pdf>, Accessed on: Dec. 8, 2019.

- [39] Cree Wolfspeed, “Six Channel SiC MOSFET Driver - CGD15FB45P1,” [Online]. Available: <https://www.wolfspeed.com/media/downloads/836/CGD15FB45P1.pdf>, Accessed on: Dec. 8, 2019.
- [40] P. D. Malliband, D. R. H. Carter, B. M. Gordon, and R. A. McMahon, “Design of a double-jacketed, closed type calorimeter for direct measurement of motor losses,” in *Proc. 17th Int. Conf. Power Electron. Variable Speed Drives (IEE Conf. Publ. No. 456)*, Sep. 1998, pp. 212–217.
- [41] A. Kersten *et al.*, “Fault detection and localization for limp home functionality of three-level NPC inverters with connected neutral point for electric vehicles,” *IEEE Trans. Transp. Electric.*, vol. 5, no. 2, pp. 416–432, Jun. 2019.
- [42] A. H. Wijenayake *et al.*, “Design of a 250 kw, 1200 V SiC MosFet-based three-phase inverter by considering a subsystem level design optimization approach,” in *Proc. IEEE Energy Convers. Congr. Expo.*, 2017, pp. 939–946.
- [43] E. Arfa Grunditz and T. Thiringer, “Electric vehicle IGBT power module sizing and drive cycle energy efficiency for various switching frequencies-based on a scalable module model,” in *Proc. 20th Eur. Conf. Power Electron. Appl.*, 2018, pp. P.1–P.10.
- [44] T. Nemeth, A. Bubert, J. N. Becker, R. W. De Doncker, and D. U. Sauer, “A simulation platform for optimization of electric vehicles with modular drivetrain topologies,” *IEEE Trans. Transp. Electric.*, vol. 4, no. 4, pp. 888–900, Dec. 2018.
- [45] A. Andersson and T. Thiringer, “Assessment of an improved finite control set model predictive current controller for automotive propulsion applications,” *IEEE Trans. Ind. Electron.*, vol. 67, no. 1, pp. 91–100, Jan. 2020.
- [46] I. P. Tsoumas and H. Tischmacher, “Influence of the inverter’s modulation technique on the audible noise of electric motors,” *IEEE Trans. Ind Appl.*, vol. 50, no. 1, pp. 269–278, Jan./Feb. 2014.
- [47] S. Haghbin, T. Thiringer, M. Alatalo, and R. Karlsson, “An LCL filter with an active compensation for a fast charger station,” in *Proc. IEEE Int. Conf. Environ. Elect. Eng. IEEE Ind. Commercial Power Syst. Eur.*, 2017, pp. 1–5.
- [48] H. Muhsen, S. Hiller, and J. Lutz, “Three-phase voltage source inverter using SiC MosFets â design and optimization,” in *Proc. 17th Eur. Conf. Power Electron. Appl.*, 2015, pp. 1–9.
- [49] J. Gottschlich, M. Kaymak, M. Christoph, and R. W. De Doncker, “A flexible test bench for power semiconductor switching loss measurements,” in *Proc. IEEE 11th Int. Conf. Power Electron. Drive Syst.*, 2015, pp. 442–448.
- [50] R. Saidur, S. Mekhilef, M. B. Ali, A. Safari, and H. A. Mohammed, “Applications of variable speed drive (VSD) in electrical motors energy savings,” *Renewable Sustain. Energy Rev.*, vol. 16, no. 1, pp. 543–550, 2012.



**Alessandro Acquaviva** (Student Member, IEEE) received the double M.Sc. degree in electric power engineering from Politecnico di Torino and KTH, Stockholm, Sweden, in 2012. He is currently working toward the Ph.D. degree in electric power engineering at Chalmers University of Technology, Gothenburg, Sweden.

His areas of interest include the modeling, control and design of electrical machines and power electronics with focus on automotive applications.



**Artem Rodionov** (Student Member, IEEE) received the M.Sc. degree in electric power engineering in 2016 from the Chalmers University of Technology, Gothenburg, Sweden, where he is currently working toward the Ph.D. degree in integrated electric drives.

His areas of interest are electrothermal design of power electronics as well as multiphase drives and machines for automotive applications.



**Anton Kersten** (Student Member, IEEE) received the B.Eng. degree in electrical engineering (major in electric power engineering) from the RheinMain University of Applied Sciences, Wiesbaden, Germany, in 2015, and the M.Sc. degree in electrical engineering (major in electric power engineering) in 2017 from the Chalmers University of Technology, Gothenburg, Sweden, where he is currently working toward the Ph.D. degree.

Since 2017, he has been with the Division of Electric Power Engineering, Chalmers University of Technology, where he is involved in the field of multilevel inverter for vehicles’ powertrain.



**Torbjörn Thiringer** (Senior Member, IEEE) received the M.Sc. and Ph.D. degrees in electric power engineering from the Chalmers University of Technology, Gothenburg, Sweden, in 1989 and 1996, respectively.

He is currently with the Chalmers University of Technology as a Professor in Applied Power Electronics. His areas of interest include the modeling, control and grid integration of wind energy converters into power grids as well as power electronics and drives for other types of

applications, such as electrified vehicles, buildings, and industrial applications.



**Yujing Liu** (Senior Member, IEEE) received the B.Sc., M.Sc., and Ph.D. degrees in electrical engineering from the Harbin Institute of Technology, Harbin, China, in 1982, 1985, and 1988, respectively.

From 1996 to 2013, he was with ABB Corporate Research, Västerås, Sweden. Since 2013, he has been a Professor of Electric Power Engineering with the Chalmers University of Technology, Gothenburg, Sweden. His research interests include motors, converters, wireless

charging for electric vehicles, generators, and power electronics for tidal power conversion and high-efficiency machines for energy saving in industrial applications.

Dr. Liu is a member of the Swedish Standard Committee on Electrical Machines.